Thermally activated avalanches: Jamming and the progression of needle domains

E. K. H. Salje, X. Ding, Z. Zhao, T. Lookman, and A. Saxena

Phys. Rev. B **83**, 104109 — Published 25 March 2011

DOI: 10.1103/PhysRevB.83.104109

Thermally activated avalanches: jamming and the progression of needle domains

E.K.H. Salje [1,2], X. Ding[1,3], Z. Zhao[3], T. Lookman[1], and A. Saxena[1]

[1]Theoretical Division and Center for Nonlinear Studies, Los Alamos National Laboratory, Los Alamos, New Mexico 87545, USA

[2]Department of Earth Sciences, University of Cambridge, Cambridge CB2 3EQ, UK

[3]State Key Laboratory for Mechanical Behavior of Materials, Xi'an Jiaotong University, Xi'an 710049, China

Large scale computer simulations of a simple model with a square lattice topology, a small shear deformation (4° shear angle) and open (free) boundary conditions show that domain boundary movements under adiabatic strain deformation lead to Vogel-Fulcher behavior at high temperatures. The activation energy is independent of temperature and details of the twin patterns. Below the Vogel-Fulcher temperature, no thermal activation was found and the time evolution of the domain pattern becomes athermal. The movement of domain boundaries is now dominated by the nucleation and growth of needle domains. Their movement occurs in fast jerks. The probability to observe jerks follows a power law spectrum with energy exponents close to $\alpha \approx 2$. At even lower temperatures, the boundary kinetics becomes erratic even in our large (one million atoms) system. The lateral movement of twin walls is found for our thin twin walls (w = 3 layers) to operate by kinks which propagate along the twin wall. The needle domains nucleate either from the surface or from other existing twin walls. Intersections of twin walls constitute pinning centers which impede the free movement of the kinks in the walls. These intersection points act then as a pattern of intrinsic, self-induced defects which lead ultimately to the power law distribution of the crackling noise of the domain walls.

PACS numbers: 81.30.Kf, 64.70.Nd, 05.50.+q, 75.10.Hk

I. INTRODUCTION

The kinetic process of front propagation of ferroic, multiferroic, and martensitic materials can be smooth, jerky or combine both aspects [1–6]. It can also be athermal or thermally activated [7–9]. Smooth propagation is understood as a feature of solitary waves (or domain walls) [10–15] while the experimental observation of jerks is somewhat surprising. Major advances came from the analysis of acoustic emission (AE) experiments which were seen as indication for avalanches and were analyzed as power laws, automata, etc [5,16–19]. While the AE and elastic three-point-bending experiments [20] have been instrumental in defining jerky interfacial behavior, both methods fail to generate a full picture of the front propagation, namely the coexistence of smooth fronts and jerks, and thermally activated movement and athermal avalanches. In magnetic systems, Barkhausen noise shows a similar characteristic [21]. As the disorder is decreased, one finds a transition from a smooth hysteresis loop to loops with a sharp jump in magnetization and avalanches in a large region around this transition point. The avalanches then show power law distributions. The theoretical approaches have, naturally, focused on the universality of the avalanche dynamics. Since the early work of Bak [22,23], Nattermann [5,24,25] and others, a multitude of renormalization studies [26,27], simulations and basic physical considerations [28–30] have elucidated this aspect.

The application to the field of ferroic phase transitions was much less elaborated besides some work on the role of the Larkin length [31,32], the roughening transition and their importance for the formation of avalanches. The Larkin length describes directly the ability of twin walls to meander in order to capture as many defects as possible inside the walls. This increases pinning of walls, i.e. systems with short Larkin length pin more strongly while pinning is much weaker in materials with long Larkin length. Meandering requires local bending of twin walls, which is strongly impeded by highly anisotropic elastic forces in ferroelastic and martensitic materials. Electron-microscopic observations have shown that weak bending of twin walls is possible in such materials while the Larkin length remains large compared with the length of the crystallographic unit cells [33]. The movement of such twin walls with very weak bending is described in this paper.

The general term crackling noise described the approach to multitudes of jerks in extended systems very aptly [28]. An important result from previous work [30] on such crackling noise is that near zero temperature and at a critical point the energy distribution of the jerks follows a power law with $P(\omega) \sim \omega^{-1/\sigma\nu z}$ where $1/\sigma\nu$ is the fractal dimension d_f of the avalanche size and z relates to the correlation length ξ with the characteristic avalanche duration $t \sim \xi^z$. Equally the size exponent and duration exponent have been derived in several models. These results are hard to compare with experimental observations in ferroelastic and multiferroic materials, however. We will show below that the elementary jerk is related to the advancement of a needle or a kink in a wall, which interacts with other needles and kinks. The interatomic interactions are highly anisotropic so that results from simulations in models such as isotropic Random Field Ising models are not realistic for ferroic materials. It also appears that the Larkin length of such elastic systems is very long and bending of interfaces requires large energies which are usually not involved in the formation of jerks [34]. In addition, we have no easy possibility of picking up demagnetization signals, as in Barkhausen noise spectra, so that the determination of size distributions of avalanches becomes very difficult. The most reliable way forward appears to be to measure the energy (Gibbs free energy or potential energy) of a ferroic system and estimate relative changes in the energy content of jerks and avalanches[1]. Most importantly, renewed emphasis was put on the temperature effect [35] which we will explore in this paper.

All this begs the following question: are all jerks also avalanches? Are experimentally observed jerks the fundamental kinetic events for crackling noise or, alternatively, can jerks be thermally activated, isolated and unrelated to collective behavior? An even more extreme scenario may be true, namely that jerks in highly defective materials and at sufficiently low temperatures lead to crackling noise (with a power law distribution of energy jumps) while jerks in materials with low defect concentrations and perhaps slightly higher temperatures masquerade as avalanches but may be simply propagating fronts in systems with finite size or finite diameter of grain boundaries.

Some indications for the possible answers stem from three key experimental

observations that have motivated these studies of avalanches and front progression: firstly, the coexistence of both types of excitations in the measurement of the heat flux during the martensitic phase transition in CuZnAl[1]. The second observation is that a single needle domain displays crackling noise together with thermally activated front propagation[2]. Thirdly, one finds power law dynamics in DMA (dynamical mechanical analysis), RUS (resonance ultrasonic spectroscopy) experiments and in AE [3–5,16–19], over some extended interval (two or more decades). The measured exponents and some theoretical predictions cluster around characteristic values, namely 1.3 for the size distribution (Ref.28 and references given there) and about 2 for the energy distribution [1,28,36,37]. The question can now be asked whether all jerks are defect generated avalanches and whether athermal behavior is required to generate such avalanches. We will show that this is not necessarily the case. At moderate temperatures we find jerky behavior which displays classic power law exponents without any extrinsic defects while jerks can be thermally activated at high temperatures.

II. THE MODEL

Our simulations follow the tradition of large scale simulations with open (free) boundary conditions and interatomic potentials [38–42]. Periodic boundary conditions are not used because domain boundaries often nucleate as needle domains from the crystal surface. Surface relaxations play a major role in the determination of the time evolution of twin walls. A typical singular case for the movement of a jerky domain wall would be a simple nucleation of a needle domain and its propagation until it hits the opposite surface. Obviously, such jerks cannot be seen in simulations using periodic boundary conditions. The computer code LAMMPS was used with an NVT ensemble.

The model is based on interatomic interactions [43] rather than force field simulations [44] because the elementary step leading to advancement of twin boundaries is known to be -- for narrow twin boundaries -- related to the sideways movement of kinks inside the boundary [45]. Kink propagation was previously observed in the propagation of phase fronts for a polytypic transition in PbI_2 but was not observed in ferroelastic materials [46]. Such atomic scale kinks are well reproduced by atomic scale

simulations while force field calculations average over such finer structural details [46].

The interatomic potentials were chosen to reproduce most closely the macroscopic Landau potentials of the relevant materials [10-12,33]. It was found that in ferroelastic materials the macroscopic Gibbs free energy follows closely a Landau potential[10]. In addition, similar Landau potentials were found recently also in martensitic phase transformations and used for simulations [47-55]. The following requirements are posed for our potential: (1) The groundstate of the model has to be a slightly sheared pseudo-cubic lattice, *i.e.,* a heavily twinned crystal would have an apparent, overall cubic symmetry but is non-cubic within any domain. (2) The length scales of the interfaces have to be of the order of three atomic repetition units. The shear angle of ferroelastic materials[10] is typically below 4^o while martensitic materials have often larger shear angles. We decided to construct the model such that the shear angle was fixed to 4^o which appears to be a good compromise for metallic and oxide materials. The shear angle is determined by the diagonal springs in the square configuration (Fig.1) which was chosen to mimic the observed Landau potentials. The thickness of the interface and the surface relaxations are determined by the competition of springs between nearest neighbors and next nearest neighbors in the direction perpendicular to the twin boundary [56]. The resulting potential is a sum of nearest neighbor interaction (short black lines in Fig.1), $U(r) = 20(r - 1)^2$, next nearest neighbor interaction (diagonal in the square lattice, heavy lines, yellow and orange online in Fig.1), $U(r) = -10(r - \sqrt{2})^2 + 2000(r - \sqrt{2})^4$, and third nearest neighbor interaction (long black lines in Fig.1), $U(r) = -(r - 2)^4$, where r is the distance vector.

The ground state of this lattice is sheared with a shear angle determined by the diagonal interaction. In addition, free boundary relaxations enhance the shear angle [57] to 4°. The calculated cell has one million particles and contains two buffer layers on top and bottom of the two-dimensional sheet. These buffer layers were sheared by the external boundary conditions (fixed shear angle, hard boundary conditions). Limited computer power leads to simulations in two dimensions. We believe that this choice is reasonable because it was shown previously that the addition of further layers did not change the microstructures significantly [12,39].

The initial condition contained one horizontal twin boundary (Fig. 2a) which under external strain moved laterally so that the final situation was a single crystal. Each configuration was annealed before any strain was changed as boundary condition for 10^6 time steps using a conjugate gradient refinement procedure to find the optimal position for each lattice point. In all cases the only relaxations which occurred during this procedure were surface relaxations, no further microstructures developed. After this relaxation, the external strain was increased via a global shear of the two boundary layers. The increase of the shear was performed adiabatically with 10^7 time steps. For comparison, the phonon excitation (vibration) time was 1000 time steps. The thickness of the initial, relaxed twin walls was three lattice units. For the analysis of the energy evolution of the domain configurations, the sum of all potential energies for all sites was calculated and recorded for each time step during the shearing of the sample.

III. RESULTS

The increase of external strain leads to the nucleation and growth of needle domains and the sideways movement of the central twin boundary. The initial nucleation site for the needle domains lies at the surface. As shear is applied at the top from right to left and at the bottom from left to right in the present calculation (Fig.2a), needles nucleate on the bottom-left surface and generate a deformation of the surface area with the needle tip oriented towards the interior of the sample. Further loading drives the needle domain from the left to the right (similar to as shown in Fig. 3e). The colors in the online version indicate the local shear where for small angles the value is additive, and is defined as $\theta = |\theta_{ver} - 4| + \theta_{hor}$. Here, θ_{ver} and θ_{hor} denote the local shear angle in the vertical direction and horizontal direction, respectively, which are calculated over three atoms, see scale in the online version). This leads to an increase of the region with right shear at the expense of regions with left shear. The movement is akin to a weaving pattern and leads to a global movement of walls from the bottom to the top [45]. During the above process, the central twin boundary remains pinned by the pre-existing needle domain and cannot move down.

After a number of needle domains and twin boundaries are nucleated, a complex wall configuration is formed in the bottom region, and hence induces the nucleation of secondary needles perpendicular to the first generation of needles (hereafter called vertical twins). As show in Fig. 2b, three domains are separated by two twin boundaries. The twin boundary between the bottom domain and the middle domain is relatively thin whereas a multitude of topological defects occur at the upper boundary. A trace of a vertical wall (in red) is seen near the right hand side of the image (A in Fig.2b). A kink in the horizontal twin boundary is pinned near the junction B in Fig.2b. This kink has a thicker wall on the left side and a thinner wall on the right side. The kink moves to the left and thereby moves the upper twin boundary downwards. Just below this configuration is a double kink (C in Fig.2b) which connects two walls. This kink moves to the right and eliminates some left sheared region.

On further loading, the vertical twins grow and finally intersect with the horizontal twins (Fig.3a-3d). The intersections of the horizontal and vertical needles and twin walls generate perturbations of the twin boundaries, which act as pinning centers for moving kinks and additional needle domains. This configuration constitutes the jamming process of the wall propagation. Following, the sideways movement of the central twin boundary occurs via the development of kinks in the twin boundary and the movement of these kinks along the twin boundary (Fig 3a-3d). All movements of the walls are related to wall segments, which move horizontally. Freely moving kinks are shown in Figs.3b, 3d-left corner and 3e, while a pinned kink is seen on the right hand side of Fig.3d. The pinning in Fig.3d occurs again at the intersection between a horizontal wall and a vertical wall. Movies on the evolution of twins at different temperatures have been attached as EPAPS (Document No.1-4) [58].

We now describe the time evolution of the total potential energy P_e of the system. After the initial relaxation the ground-state potential energy of the system is -0.026721 in normalized units, at zero temperature. When the shear increases the potential energy increases quadratically with the macroscopic shear strain. After a threshold for the nucleation of a twin boundary is surpassed, a domain boundary propagates and reduces the strain energy. Accordingly the potential energy reduces

stepwise (on the timescale of the needle propagation). Further increase of the shear strain repeats the same process with further domains propagating. This leads to a saw tooth appearance for the energy derivative versus strain plots in Fig.4a. Temperature does superimpose dynamical fluctuations at high temperatures which ease the nucleation and growth of needle domains and the propagation of the kinks inside the twin domain walls. Visual inspection of the graphs on the left hand side of Fig 4 already shows that we can distinguish three dynamical regimes: at high temperatures we find significant thermal fluctuations and a very large number of energy jerks. In the intermediate temperature regime, a large number of jerks still persist but with very few temperature fluctuations while at low temperatures the initial, mechanical saw-tooth pattern is clearly visible with few additional jerks. We now quantify these temperature regimes.

The potential energy versus shear strain curves in Fig. 4 are now analyzed in terms of jerk energies. As the potential energy is the integral over all energy contributions by moving twin boundaries, we resort to measurements of the squared first derivative of P_e with respect to the applied shear strain (e_s). As the shear strain increases with a constant rate, the derivative is identical to derivatives in time. Similar derivatives were used previously [59] to derive temporal fluctuations in avalanching systems and a similar quantity, $(de_s/df)^2$ where e_s is the macroscopic shear strain and f is the applied force, was used in the experimental paper[2]. These data are shown in Figs. 4(a), (c), (e), (g), large jerks appear at the edge of the saw-teeth and smaller ones inside the ramps of each saw-tooth. We note here that the avalanches are not properly defined in the thermal case and also in the power law region close to the Vogel-Fulcher temperature. With this caveat in mind, the analysis of the derivatives appears to be the best option at present.

The probability to find a jerk of certain energy content is then plotted as a function of energy of the jerk. Here we see the three regimes very clearly on Figs. 4 (b), (d), (f) and (h): the probability distribution is exponential at high temperatures and follows closely a Vogel-Fulcher (VF) distribution $P(E) \sim \exp-[E/(T - T_{VF})]$ where T_{VF} is the Vogel-Fulcher temperature. We calibrate all temperatures with respect to T_{VF} (= 4×10^{-4}, in our potential units). This thermally activated behavior disappears when T

is less than $1.2T_{VF}$ and gives way to a power law distribution $P(E) \sim E^{-\alpha}$ dependence in the temperature regime well below $1.2T_{VF}$ (Fig.4f). In the Vogel-Fulcher regime we find a very good agreement of the distribution function with the Vogel-Fulcher law. Plotting the absolute value of the inverse exponent (normalized by T_{VF}) as a function of temperature (Fig. 5) leads to the definition of $T_{VF.}$ At a slightly higher temperature of 1.2 T_{VF} we find that the exponential distribution is already significantly perturbed while a power law fit is valid only over a very small interval. We define this temperature as the cross-over point between the Vogel-Fulcher regime and the power-law regime. At lower temperatures we find the power law regime in the interval II. The horizontal line indicates the upwards shift of the x-axis if one takes the 1.2 T_{VF} as the crossover point.

IV. DISCUSSION

Vogel-Fulcher relaxational behavior is typically observed in glassy systems and systems which undergo relaxor phase transitions [60]. T_{VF} is often called the freezing temperature at which all dynamical relaxations cease. It is commonly believed that the dielectric response of glasses and relaxor materials is governed by the ensemble of local configurations which relax dynamically with an exponentially broad spectrum of relaxation times. For relaxation spectra which are smooth and wide enough, the real part of the dielectric permittivity can be approximated by the following logarithmic scaling:

$$\varepsilon(\omega, T) = \varepsilon_0(T)\, f(\ln \omega_0 / \omega, T) .$$

The maximum of $\varepsilon(\omega, T)$ may occur at T_A so that the T_{VF} can be approximated by

$$T_{VF} = T_A + C\,(\ln \omega_0 / \omega),$$

with some constant C which describes the dispersion of the relaxation times [61]. Logarithmically slow relaxations and temperature dependences of the VF type are hence conceptually linked [62] and have been explored widely for highly disordered systems [63]. Our results for the power law distribution at modest temperatures just below T_{VF} show power law behavior with exponent $\alpha \approx 2$ which is identical to those one would expect for avalanche statistics with large defect concentrations[64]. This clearly shows that the empirical observation of power law distributions with α near 2 does not imply that defect generated crackling noise or critical avalanches or

self-induced criticality is at play. No extrinsic defects are part of our model so that the only reason why jerky front propagation follows a power law distribution appears to be that the active centers of the movement, namely the twin boundaries, generate the defects intrinsically. This means that at a well-defined wall concentration their interaction leads to jamming and hinders further time evolution of the strain release. Close inspection of the domain pattern in Fig.3 shows that the active defects are the intersections between walls and the tips of needle domains. Parallel twin walls do (virtually) not interact over distances relevant in our patterns so that the network of interacting centers is defined by the points (or lines in three dimensions) of intersections of walls. The intersections form a fairly high defect density which would satisfy the usual conditions of avalanche dynamics. We can then characterize our results as follows: the defect concentration is too low at low temperatures to generate smooth jerk distributions. At slightly higher temperatures, these concentrations are sufficient and power law distributions are seen. The energy exponent assumes values around 2. At temperatures well above the Vogel-Fulcher temperature we find thermally activated behavior with constant activation energies.

ACKNOWLEDGMENTS

We are grateful to CNLS (Center for Nonlinear Science) and the US DOE at LANL (DE-AC52-06NA25396) for support. XD and ZZ appreciate the support of NSFC (50771079 and 50831004), the 973 Program of China (2010CB631003) and 111 project (B06025).

References

1. M. C. Gallardo, J. Manchado, F. J. Romero, et al.; Phys. Rev B, **81**,174102 (2010).
2. R. J. Harrison and E. K. H. Salje; Appl Phys. Lett; **97**, 021907 (2010).
3. E. K. H. Salje, H. Zhang, H. Idrissi, et al.; Phys Rev. B; **80**,134114 (2009).
4. E. K. H. S alje, J. Koppensteiner, M. Reinecker, et al.; Appl. Phys.Lett. **95**, 231908 (2009).
5. L. Carrillo, L. Manosa, J. Ortin, et al.; Phys. Rev. Lett., **81**, 1889 (1998).
6. F. J. Romero, M. C. Gallardo, S. A. Hayward, et al.; J. Phys.:Condensed Matter; **16**, 2879 (2004).
7. T. Kakeshita, K. Kuroiwa, K. Shimizu et al.; Mat. Trans. **34**, 423 (1993).
8. A. G. Khatchaturyan, S. M. Shapiro and S. Semenovskaya; Phys. Rev. B, **43,** 10832 (1991).
9. L. Bataillard, J. E. Bidaux and R. Gotthard; Phil. Mag. A, **78,** 327 (1998).
10. E. K. H. Salje, Phase Transitions in ferroelastic and co-elastic crystals, Cambridge University Press **(1993)**, Cambridge, UK.
11. A. E. Jacobs; Phys. Rev. B, **61**, 6587 (2000).
12. E. Salje and K. Parlinkski; Supercond. Sci. Technol., **4**, 93 (1991).
13. J. Novak and E. K. H. Salje; Europ. Phys. J. B, **4**, 279 (1998).
14. W. Vansaarloos and P. C. Hohenberg; Physica D, **56,** 303 (1992).
15. G. T. Dee and W. Vansaarloos; Phys. Rev. Lett., **60**, 2641 (1998).
16. E. Vives, J. Ortin, L. Manosa, et al,; Phys. Rev. Lett., **72**, 1694 (1994)
17. F. J. Perez-Reche, E. Vives, L. Manosa, et al.; Phys. Rev. Lett., **87**, 195701 (2001).
18. F. J. Perez-Reche, B. Tadic, L. Manosa, et al.; Phys. Rev. Lett., **93**, 195701 (2004).
19. F. J. Perez-Reche, F. Casanova, E. Vives, et al.; Phys. Rev. B, **73**, 014110 (2006).
20. E. K. H. Salje, J. Koppensteiner, M. Reinecker, et al.; Appl. Phys. Lett., **95**, 231908 (2009).
21. K. A. Dahmen, J. P. Sethna, M. C. Kuntz and O. Perkovic; J Magnetism and Magnetic Materials **226**, 1287 (2001).
22. M. Paczuski, S. Maslov and P. Bak; Phys. Rev. E, **53** 414 (1996).
23. M. Paczunski, S. Maslov and P. Bak; Europhys. Lett., **27** (1994) 97.
24. T. Nattermann; Phys. Rev. Lett., **64**, 2454 (1990).
25. T. Nattermann, Y. Shapir and I. Vilfan; Phys. Rev. B, **42**, 8577(1990).
26. J. Feder; Fractals (Plenum, New York, 1889).
27. D. S. Fisher, Physics Report **301**, 113 (1998).
28. J. P. Sethna, K. A. Dahmen and C. R. Myers; Nature, **410**, 242 (2001).
29. K. Dahmen and J. P. Sethna; Phys. Rev. B, **5**3, 14872 (1996).
30. M. C. Kuntz and J. P. Sethna; Phys. Rev. B, **62**, 11699 (2000).
31. L. Proville; J. Stat. Phys., **137**, 717 (2009).
32. C. Caroli and P. Nozieres; Europ. Phys. J. B, **4**, 233 (1998).
33. E. K. H. Salje; CHEMPHYSCHEM, **11**, 940 (2010).
34. E. K. H. Salje and Y. Ishibashi; J. Phys.: Condensed Matter, **8**, 8477 (1996).

35. R. A. White, Y. Liu and K. A. Dahmen; Europ. Phys. Lett., **86**, 50001 (2009).
36. L. A. N. Amaral and K. B. Lauritsen; Physica A, **231**, 608 (1996).
37. V. Frette et al.; Nature **379**,49 (1996).
38. K. Parlinski, E. K. H. Salje and V. Heine; Acta Metallurgica et Mat. **41**, 839 (1993)
39. S. Conti and E. K. H. Salje; J. Phys.: Condensed Matter **13**, L847 (2001).
40. J. Novak and E. K. H. Salje; Europ. Phys. Journal B **4**, 279(1998); J. Novak and E. K. H. Salje; J. Phys.: Condensed Matter **10**, L359 (1998).
41. A.M. Bratkovsky, S. C. Marais, V. Heine et al.; J. Phys.: Condensed Matter **6**, 3679 (1994); A. M. Bratkovsky, E. K. H. Salje, S. C. Marais, et al.; Phase Transitions **48**, 1 (1994).
42. V. Yamakov, D. Wolf, S. R. Phillpot et al.; Nature Materials, **3**, 43 (2004).
43. J. K. Deng, X. D. Ding, T. Lookman, et al.; Phys. Rev. B, **81**, 220101 (2010).
44. M. Porta, T. Castan, P. Lloveras, T. Lookman, et al.; Phys. Rev. B, **79**, 214117 (2009); R. Groger, T. Lookman and A. Saxena; Phys. Rev. B, **78**, 184101 (2008).
45. E. Salje, B. Palosz, B. Wruck; J. Phys.: Condensed Matter, **20**, 4077(1987); A. Froseth, H. Van Swygenhoven and P. M. Derlet; Acta Mat. **52**, 2259 (2004).
46. G. Boussinot, Y. Le Bouar and A. Finel; Acta Mat. **58**, 4170 (2010); A. Gaubert, Y. Le Bouar, and A. Finel; Phil. Mag. **90**, 375 (2010).
47. E. K. H. Salje, H. Zhang, A. Planes, et al.; J. Phys.:Condensed Matter, **20**, 275216 (2008).
48. H. Zhang, et al.; J. Phys.:Condensed Matter **20**, 055220 (2008).
49. E. K. H Salje, H. Zhang, D. Schryvers, et al.; Appl. hys. Lett., **90**, 221903 (2007).
50. V. Berti, M. Fabrizio and D.Grandi, J. Math. Physics, **51**, 06290 (2010).
51. P. Lloveras, T. Castan, M. Porta, et al.; Phys. Rev. B, **80**, 054107(2009).
52. A. Umantsev, Physica D **235**, 1 (2007).
53. M. Arndt, M. Griebel, V. Novak, et al.; Int. J. Plasticity **22**, 1943 (2006).
54. J. Khalil-Allafi, W. W. Schmahl and T. Reinecke; Smart Mat. and Structures **14**, S192 (2005).
55. A. E. Jacobs, S. H. Curnoe and R. C. Desai, Mat. Trans. **45**, 1054 (2004); A. E. Jacobs, S. H. Curnoe and R. C. Desai; Phys. Rev. B, **68**, 224104 (2003)
56. E. K. H. Salje, J. Phys.: Condensed Matter, **20**, 485003 (2008).
57. J. Novak, U. Bismayer and E. K. H. Salje; J. Phys.: Condensed Matter, **14**, 657 (2002) ; W.T. Lee, M. T. Dove., and E. K. H. Salje; J. Phys.: Condensed Matter **12**, 9829 (2000); W. T. Lee, E. K. H. Salje and M. T. Dove, J. Phys.: Condensed Matter **11**, 7385 (1999); B. Houchmanzadeh, Lajzerowicz and E. Salje, J. Phys.: Condensed Matter **4**, 9779 (1992).
58. See supplementary material at http://link.aps.org/supplemental/ fro the movies that show the evolution of twins at different temperatures.
59. M. Rypdal and K.Rypdal; Phys. Rev. E **78**, 051127 (2008).
60. L. E. Cross; Piezoelectricity, Springer Series in materials science, **114**, 131 (2008)
61. F. Chu, N. Setter and A. K. Tagantsev; J. Appl. Phys., **74**, 5129 (1993).
62. K. Trachenko and V. V. Brazhkin; J.Phys.: Condensed Matter **21**, 425104 (2009).
63. U. Koster, J. Meinhardt, S. Roos, et al. Mat. Sci. Eng. A **226**, 995 (1997); A. E. Glazounov, and A. K. Tagantsev, Phys. Rev. Lett. **85**, 2192 (2000); X. G. Tang, J. Wang, X. X.Wang, et al. Solid State Comm. **131**,163 (2004); M. Tyunina, J. Levoska, Phys. Rev. B **63**, 224102 (2001); H.Tanaka, J. Phys.: Condensed Matter **10**, L207 (1998).

64. J. Ortin, I. Rafols, L. Carrillo, et al. J. Physique IV **5**, 209 (1995).

Figure Captions

Figure 1. The model with nearest and third nearest neighbors along the horizontal and (almost) vertical axis, the bold double arrows indicate the non-linear Landau springs. The shear angle is 4° in a box of 10^6 atoms including surface relaxations.

Figure 2. (a) The initial twin model with one central twin boundary, a shear is applied at the top from right to left and at the bottom from left to right. (b) A complex wall configuration is formed (in the bottom region of the initial model), prior to the nucleation of secondary needles perpendicular to the first generation of needles.

Figure 3. (a) Global microstructure at $T = 2.4T_{VF}$ with three horizontal penetrating twin boundaries and numerous needle domains both horizontally and vertically. The image (b) is the expanded black square region in (a) showing a typical kink formation which facilitates the lateral movement of the horizontal twin boundary. These kinks are weakly pinned (at high temperatures) by the intersection with the vertical twin boundaries. (c) and (d) show similar view for a configuration near the Vogel-Fulcher temperature ($T = 1.2T_{VF}$). The domain structure has fewer intersections; two kinks (one pinned and one free) are shown in (d). The microstructure below T_{VF} is similar to (c,d). (e) At very low temperatures ($T = 1.68\times10^{-3}T_{VF}$) only lateral movements of twin walls are found. The mechanism of the movement is exclusively via the movement of kinks inside the walls.

Figure 4. Time evolution of the microstructure at various temperatures. The energy versus strain curve (Fig. 4a) shows the typical saw-tooth behavior with superimposed noise in the derivative of the energy curves. The probability to find a jerk of a certain energy content is then plotted as a function of energy of the jerk at different temperatures is shown in b, d, f, h. These distributions show erratic behavior at very low temperatures (a, b), power spectra below the Vogel-Fulcher temperature (c, d) and thermally activated behavior at high temperatures (g, h). At $1.2T_{V\,F}$ (e, f) the spectrum shows a short cut-off for the power law with large exponential tails.

Figure 5. Inverse exponent of the logarithmic probability functions in Fig. 4 as a function of temperature. The linear dependence of the inverse slope constitutes the Vogel-Fulcher law. We normalized the temperature scale with respect to the Vogel-Fulcher temperature. At lower temperatures (regime II) the probability functions follow a power law with energy exponents around 2. At very low temperatures (regime I) our simulations do not provide sufficient data to constitute reliable functional dependences. In this regime a fairly erratic dependence is expected even in experimental observations of small samples. The letters (a)-(e) refer to the microstructures of Fig.3 that are seen in the various regimes.

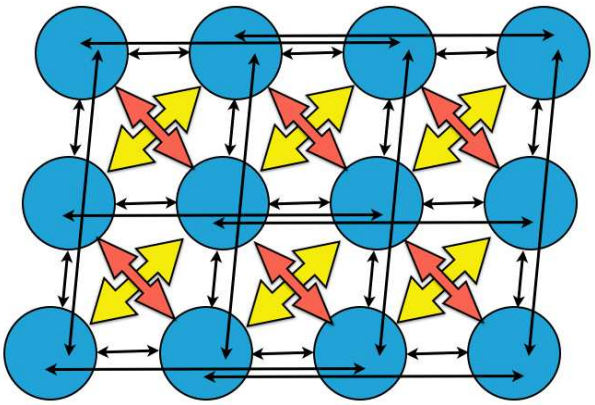

Figure 1 BW11023 03FEB2011

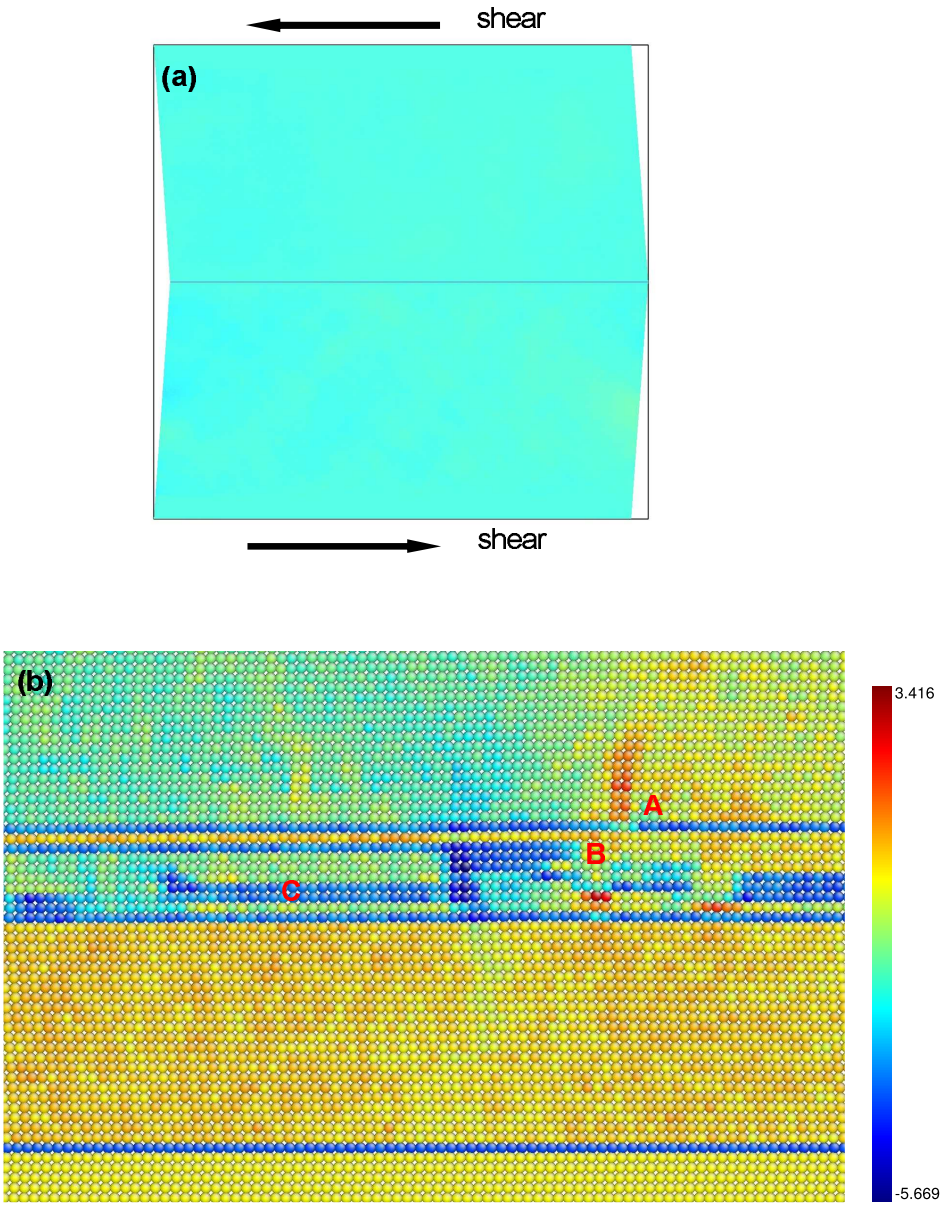

Figure 2 BW11023 03FEB2011

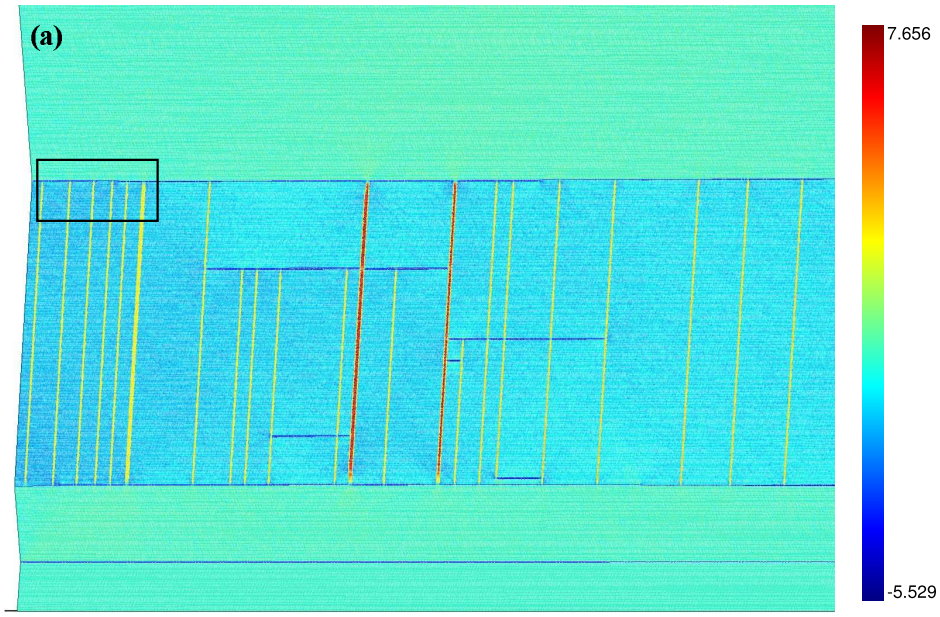

Figure 3a BW11023 03FEB2011

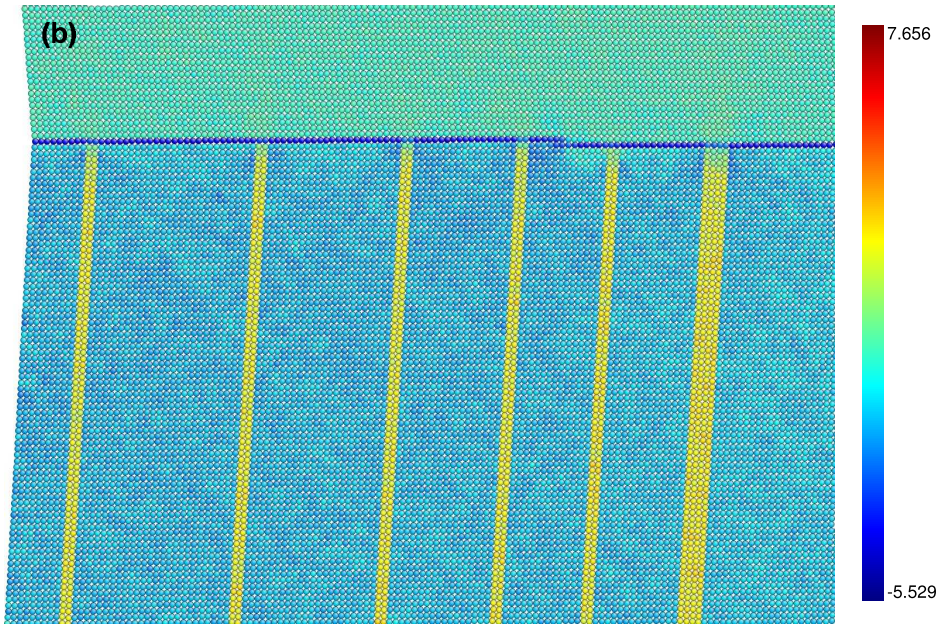

Figure 3b BW11023 03FEB2011

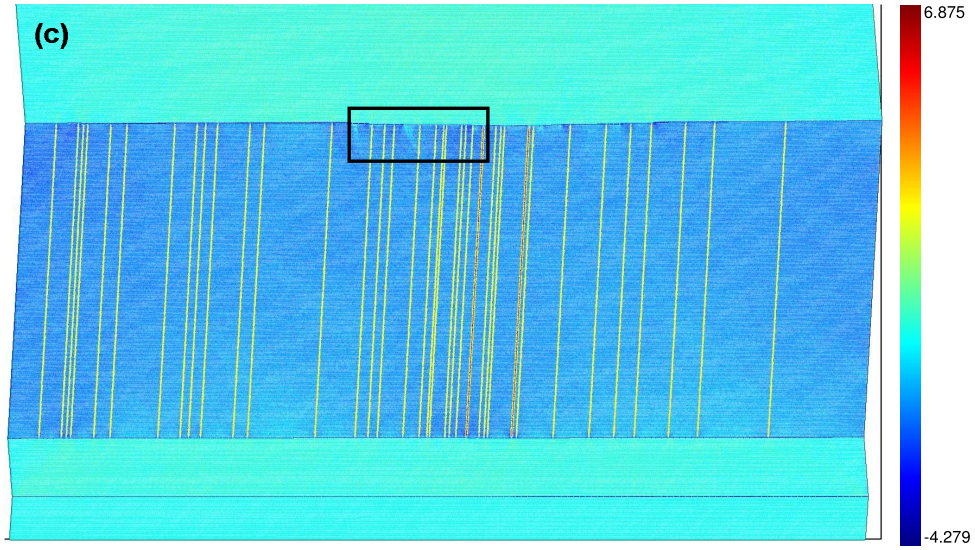

Figure 3c BW11023 03FEB2011

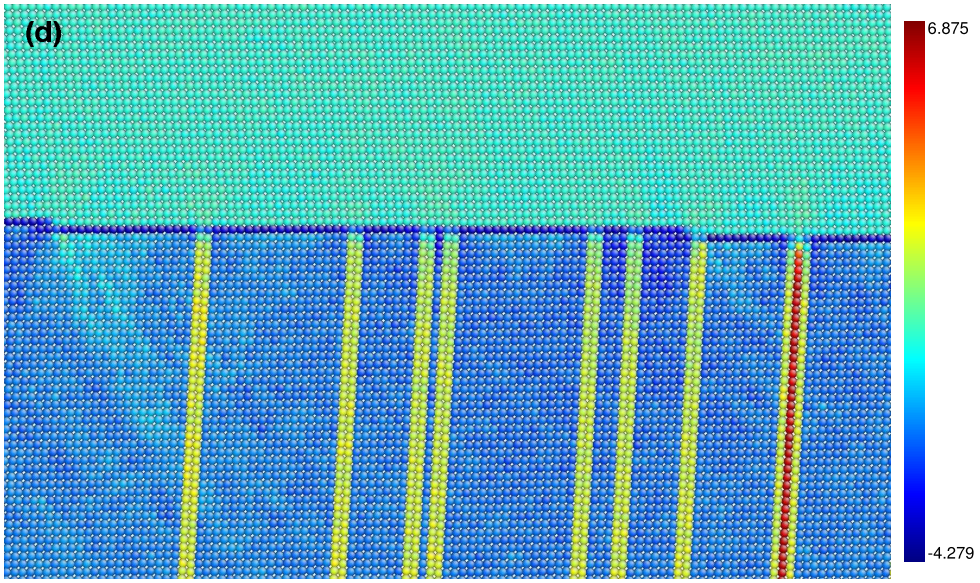

Figure 3d BW11023 03FEB2011

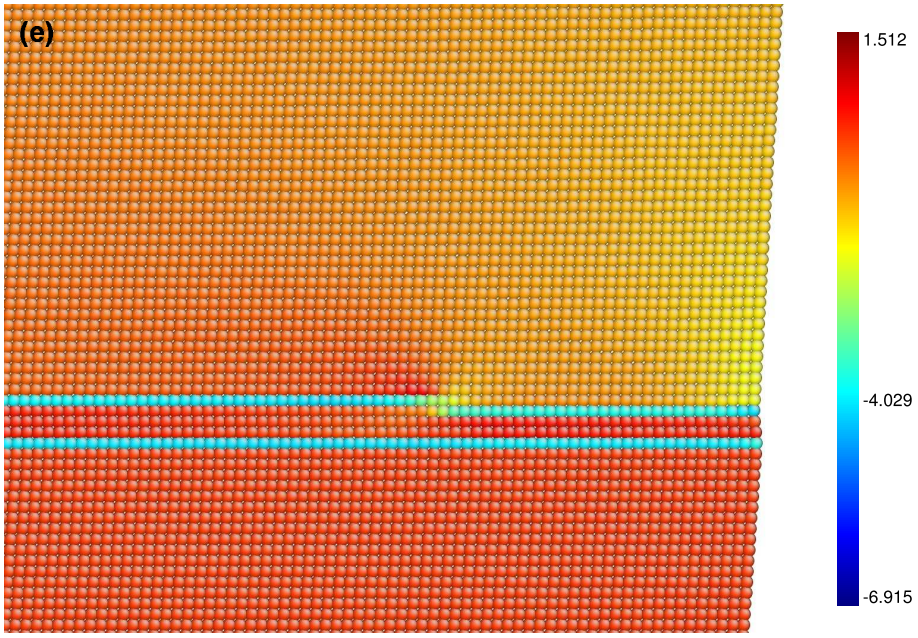

Figure 3e BW11023 03FEB2011

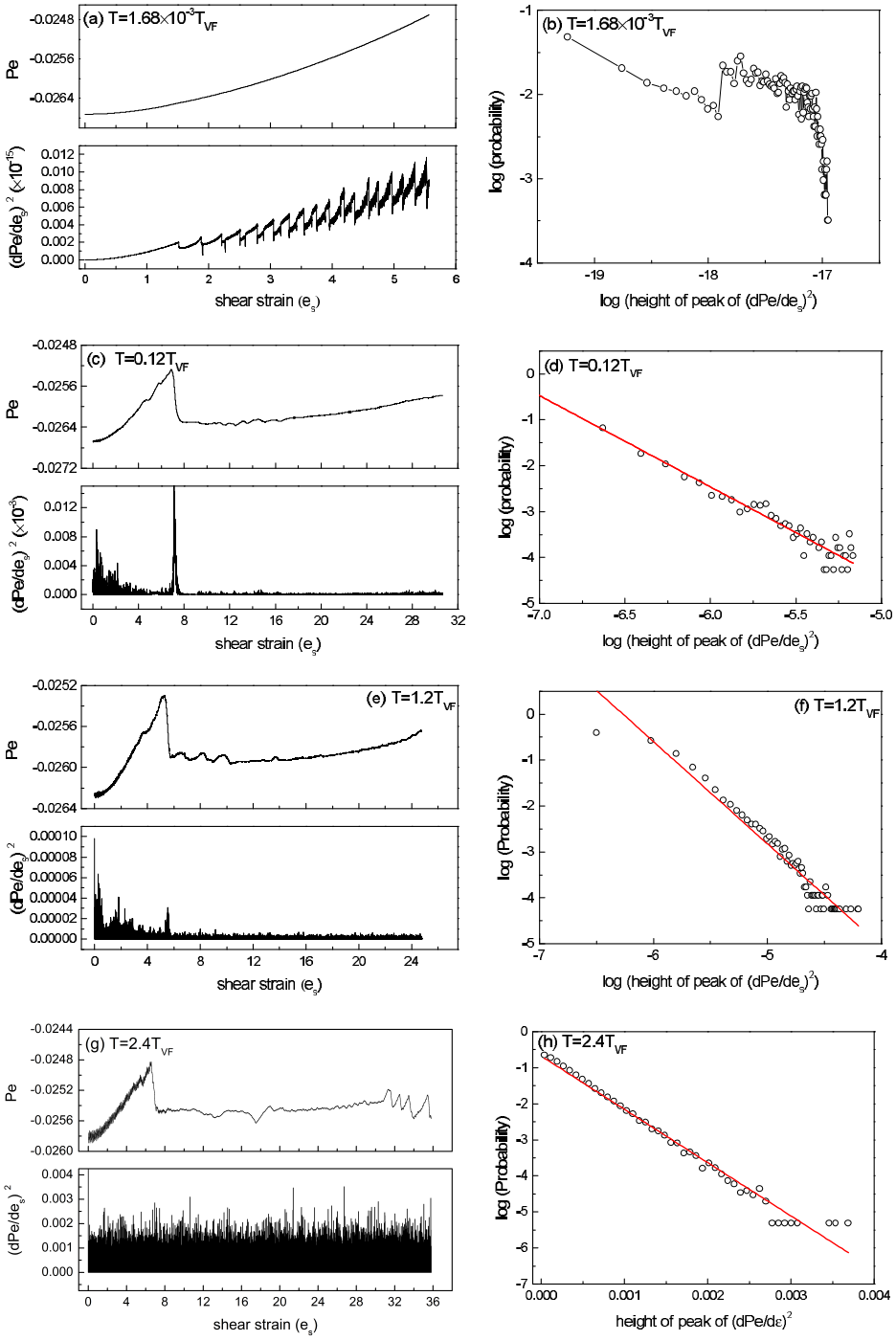

Figure 4 BW11023 03FEB2011

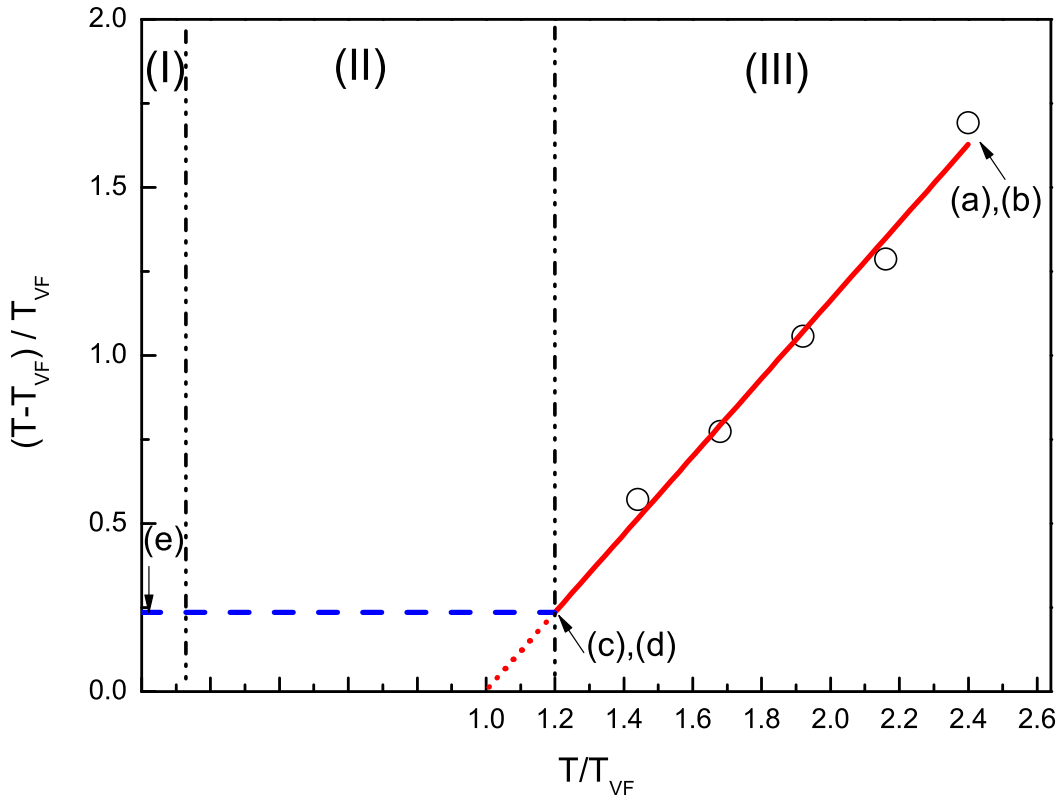

Figure 5 BW11023 03FEB2011